Technical Note

Landslides
DOI 10.1007/s10346-026-02707-y
Received: 8 July 2025
Accepted: 20 January 2026


Nicola Scarselli · Silvia Ceramicola · Giulia Magnarini

# Detrending—a new trend in geomorphology? Unravelling erosional processes at the base of submarine landslides

**Abstract** Erosion at the base of submarine landslides remains poorly understood, despite being a critical threat for the stability of valuable seabed infrastructures such as communication cables and offshore renewable energy installations. Clues about its genesis are often preserved at the basal surface of landslides in the form of elongated scours aligned in the direction of landslide transport. However, these features are commonly concealed by the overlying landslide mass, and when visible, the overprint of slope gradient often masks their structural complexity. This research applies detrending algorithms to remove slope-induced overprint from exceptionally well-imaged landslide basal surfaces mapped using high-quality 3D seismic reflection data. Detrending revealed the morphological characteristics of prominent scour fields, providing new insights into the erosional mechanisms operating at the base of submarine landslides. The results indicate that distinct basal erosion processes create morphometrically diagnostic scour features. For example, basal block tooling produces steep and symmetric scours with increased erosion depth at their downslope termination, suggesting enhanced material removal at the base of blocks as these progressively sink within a decelerating landslide. Erosion might also occur by the action of longitudinal flow vortices at the boundary layer of gravity flows, with the latter generated from the disaggregation of landslides evacuating further upslope. These scours are spatially detached from landslide headscarps and initiate where seabed irregularities ignite secondary flow vorticity. The termination of this type of scours where bathymetric breaks occur suggests changes in flow dynamics and suppression of vorticity at those locations. Recognising different scour morphologies is key to reconstructing failure dynamics and better assessing hazards posed by submarine landslides. The detrending method presented here offers a powerful tool able to unravel complex geomorphic features, with potential applications across marine, terrestrial, and planetary environments.

**Keywords** Submarine landslides · Basal erosion · Detrending · Seismic reflection

## Introduction

Submarine landslides are ubiquitous features of continental margins and play a major role in the shaping of offshore open slopes and ocean floors (Prior et al. 1984; Moscardelli et al. 2006; Butler and Turner 2010; Ogata et al. 2019; Scarselli et al. 2022; Mangano et al. 2023). Their occurrence poses threats to seabed infrastructures (Frey-Martínez et al. 2011; Lu and Shipp 2011; Wang et al. 2018; Liu et al. 2023; Ceramicola et al. 2024a) and coastal communities (Løvholt et al. 2015; Masson et al. 2006; Urgeles et al. 2019; Ceramicola et al. 2024b), the latter largely due to their tsunamigenic potential (Ceramicola et al. 2014; Harbitz et al. 2014; Tappin 2021; Ramalho et al. 2024). Understanding evacuation mechanisms—how materials are displaced and transported during a submarine landslide—is crucial for reconstructing failure dynamics and for assessing hazard potential and vulnerability, particularly in relation to tsunamis, and ultimately for mitigating associated risks.

Emplacement of submarine landslides is often accompanied by seabed erosion as observed in flume analogue models (Toniolo et al. 2004; Haas and Woerkom 2016), exposed fossil examples (Draganits et al. 2008; Dakin et al. 2013), and geophysical imaging (Fig. 1; Gee et al. 2007; Bull et al. 2009; Nugraha et al. 2022; Scarselli 2020). Erosion at the base of landslides is often accompanied by the development of elongated, linear, concave features extending from the evacuation area (source) of the failure and typically follows the direction of downslope transport (Fig. 1). These features are widely recognised in the literature and referred to with a multitude of terms: cat-claw scours (Moscardelli et al. 2006); grooves and furrows (Posamentier and Kolla 2003; Bull et al. 2009); striations (Nissen et al. 1999; Bull et al. 2009); tool marks (Sobiesiak et al. 2018), and groove casts (Draganits et al. 2008). In this contribution, all such features are referred to as scours. Although scours likely hold valuable insights into failure dynamics, their origin remains poorly understood. Their formation is often ascribed to seabed tooling caused by large, rigid blocks entrained within a moving submarine landslide. However, such blocks are not always observed, possibly due to removal during transport, or because other erosional mechanisms may also be involved (Sobiesiak et al. 2018). Additionally, challenges related to the resolution and scale of geophysical imaging combined with the frequent burial of the basal surface beneath overlying landslide deposits hinder the understanding of the processes that form them. This contribution aims to shed new light on the possible formation mechanisms of scours at the base of submarine landslides by applying detrending methods to seismic reflection data and unlock an in-depth granular analysis of these features.

Detrending is the removal of an underlying trend from a dataset allowing isolation of patterns unrelated to such a trend (Wu et al. 2007). Detrending is widely utilised in a variety of fields including economics (Watson 1986), medicine (Tanabe et al. 2002) and climate sciences (Ols et al. 2023). In geoscience, detrending has been used to remove the effect of valley slope to better understand the characteristics of river profiles on steep terrains (Brigante et al. 2017; Zhang et al. 2020). In this research, detrending is applied to enhance the morphological analysis of landslides' basal surfaces identified on three dimensional (3D) seismic reflection

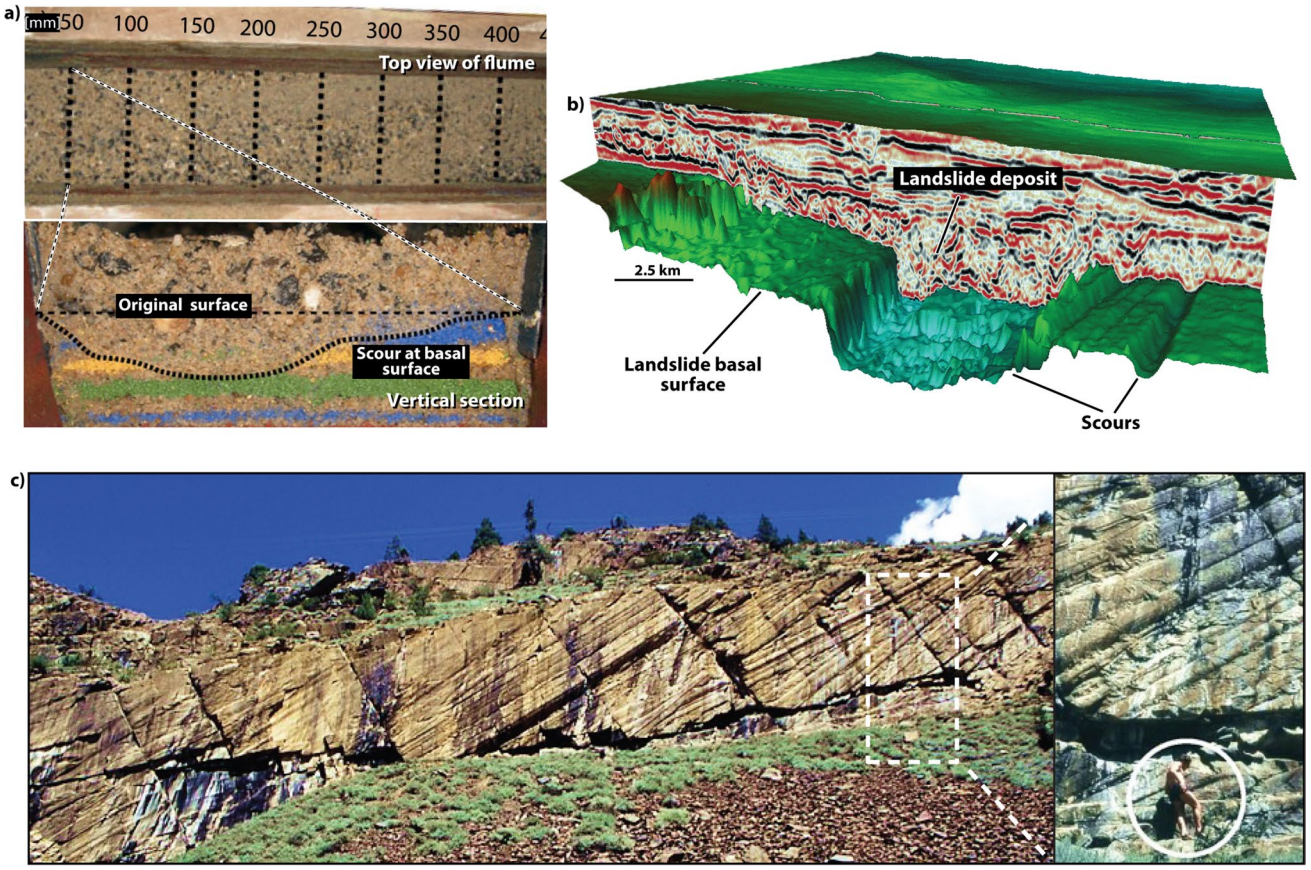


**Fig. 1** Examples of scouring at the base of landslides. **a** Picture of flume experiment showing erosion of a fixed bed by an overlying flow made of a mixture of clay, sand, and gravel (modified from Haas and Woerkom 2016). **b** 3D seismic display showing a series of elongated scours at the base of a submarine landslide (modified from Moscardelli et al. 2006). **c** Outcrop photograph of the basal surface of a submarine landslide showing intersecting, elongated scours (modified from Draganits et al. 2008). The basal surface is observed along the vertical beds exposed at the outcrop. White circle in the inset indicates the scale of the structures

data. By removing the broader bathymetric trends (i.e. regional slope) that commonly affect offshore settings, detrending enables a detailed interpretation of the basal surface geometries and associated erosional features (Fig. 2). Here, through the analysis of 3D seismic reflection data, we investigate the morphologies of the basal surface of two large-scale (> 30 km$^3$) submarine landslides exposed on the slopes of the NW Shelf of Australia (Fig. 3). Given the strong slope trend imposed by the bathymetric setting in the region (Fig. 3), detrending workflows enabled a comprehensive

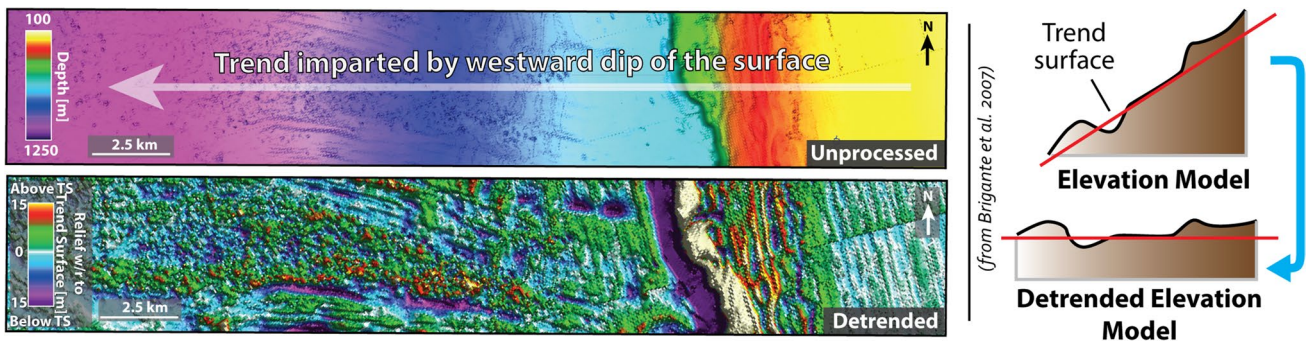


**Fig. 2** Visualisation of an unprocessed surface (top) and relative detrended surface (bottom). The detrended surface highlights intricate patterns that are poorly imaged on the unprocessed surface. The schematic diagram shows the concept of detrending whereby an elevation model exhibiting a strong dip is detrended by removing the effect of the dipping trend surface (modified from Brigante et al. 2017)

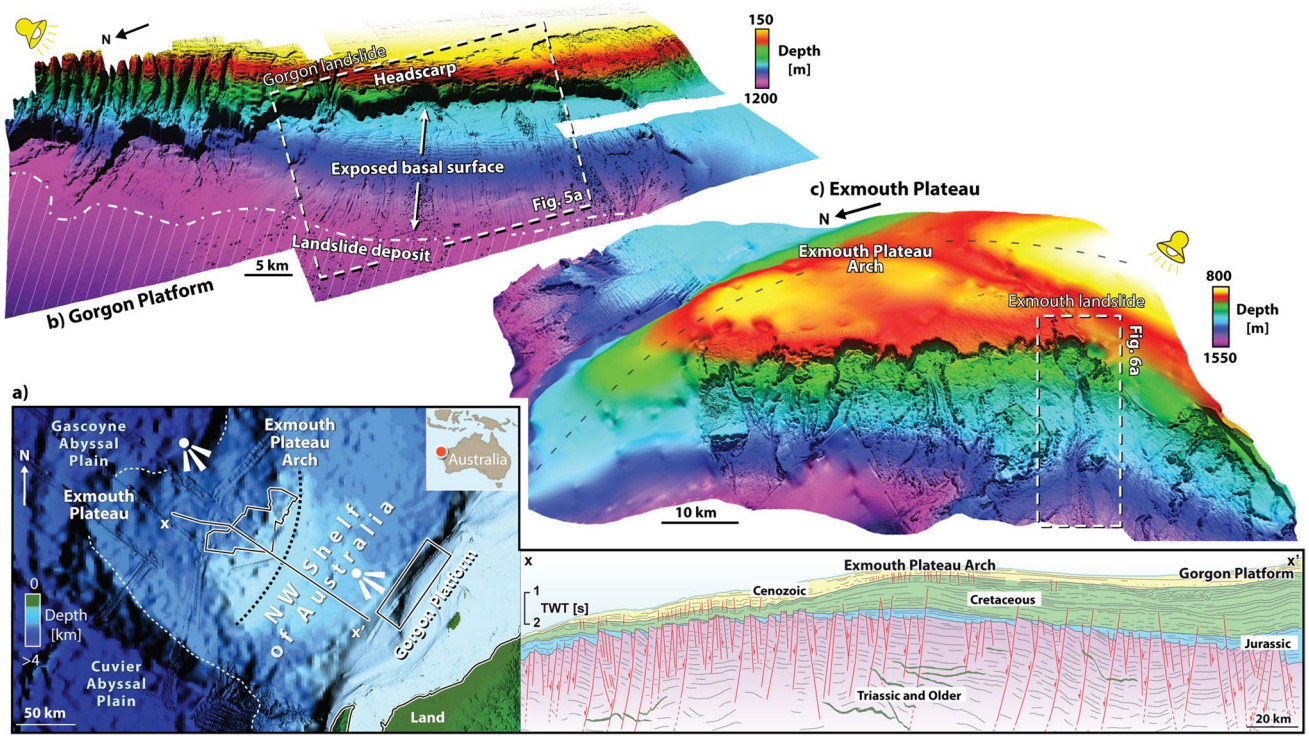


**Fig. 3** **a** Map on the left shows the location of the 3D seismic datasets within the study area. The panel to the right presents a regional seismic profile illustrating the nature of the rifted architecture of the Exmouth Plateau, North West Shelf of Australia. The landslides analysed in this paper are contained in the post-rift Cenozoic unit. Location of the regional profile is shown in the map on the left. 3D visualisations of the seabed reflection showing (**b**) the Gorgon landslide along the shelf of the Gorgon Platform and (**c**) the Exmouth landslide . The latter is found on the western flank of the Exmouth Plateau Arch, a prominent bathymetric relief located ~100 km offshore of the Gorgon Platform

morphological analysis of the basal scours, providing valuable insights into the erosional processes of the investigated submarine landslides.

## Submarine landslides occurrence in the NW Shelf of Australia

NW Australia's Continental Shelf comprises a stretched continental crust that exhibits a well-developed rift architecture within the Triassic and Jurassic sections (Fig. 3a; Longley et al. 2002; McCormack and McClay 2013; Nugraha et al. 2019; Bilal and McClay 2022; Winata et al. 2023). These rifted strata are overlain by Cretaceous and Cenozoic post-rift sediments of marine origin (Fig. 3a; Longley et al. 2002; Nugraha et al. 2022). In the Exmouth Plateau and surrounding areas (Fig. 3a), a number of shallow failures have been documented to have affected the Miocene to recent near seabed stratigraphy (Hengesh et al. 2012; Hengesh et al. 2013; Scarselli et al. 2013; Scarselli et al. 2020; Wu et al. 2021; Nugraha et al. 2022; Wu et al. 2023; Keep et al. 2024). The precise ages of these failures are unknown due to poor stratigraphic constraints within the Neogene deposits of the region (Keep et al. 2024).

Key triggering mechanisms for the activation of these landslides have been ascribed to a combination of factors such as seismicity, rapid seabed oversteepening, and the presence of weak, overpressured layers within the post-rift stratigraphic succession (Scarselli et al. 2013; Hengesh et al. 2013; Wu et al. 2023; Keep et al. 2024).

The Gorgon landslide is a large failure affecting the seabed downslope of the Gorgon Platform continental shelf, where slope angles are up to 15° (Fig. 3b; Hengesh et al. 2012; Nugraha et al. 2022). The landslide has an estimated volume of ~300 km$^3$ (Hengesh et al. 2012; Nugraha et al. 2022) and exhibits a composite headscarp located at water depth of 400 m, suggesting a failure dynamic of multiple, laterally contiguous events. The landslide has a runout of ~70 km and developed through full evacuation of the headscarp, leaving the basal surface exposed at the seabed (Fig. 3a; Hengesh et al. 2012; Nugraha et al. 2022; Riera et al. 2022).

The Exmouth landslide is located across the western slope of the Exmouth Plateau Arch, a prominent, NE-trending seabed relief feature ~100 km offshore the Gorgon Platform (Fig. 3a). This landslide is part of a series of adjacent failures documenting a history of instability across the arch spanning from the Neogene to the present day (Fig. 3a and c; Scarselli et al. 2013). The headscarp of the landslide is located at a water depth of ~800 m, along a slope with an overall regional gradient of ~1°. The landslide has an estimated volume of 30 km$^3$ and extends downslope for ~40 km (Scarselli et al. 2013). Mapping of the landslide's basal surface shows elongated, sub-parallel lineaments interpreted as scours resulting from erosion and removal of seafloor sediments as the landslide masses moved down the slope (Figs. 5 and 6; Scarselli et al. 2013).

## Data and methods

The analysis involved interpreting key surfaces of interest (i.e. landslide basal surfaces) using 3D seismic reflection data from the two study areas (Figs. 3 and 4). Given the lack of extensive multibeam coverage, the seabed reflection was interpreted from the seismic data to derive the bathymetry over the landslide areas. Further

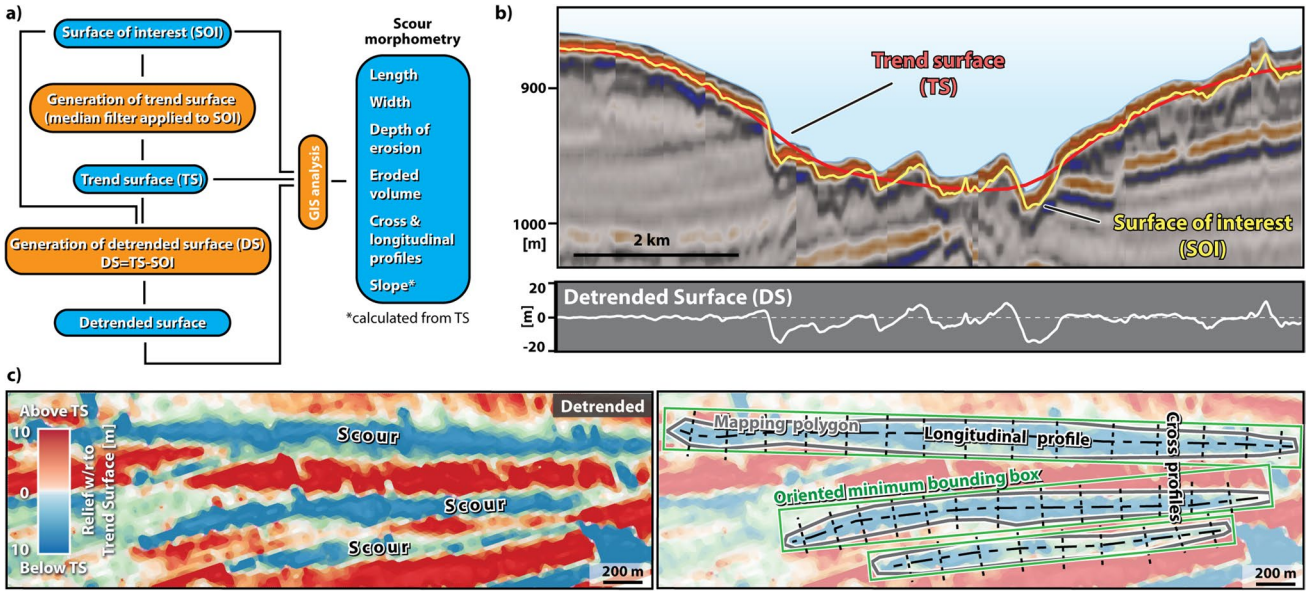


**Fig. 4** **a** Schematic workflow chart showing how the morphometric characteristics of scours at the base of landslides were analysed in the research. Note that the morphometric analysis was applied on detrended basal surfaces so as to remove the effect of slope. This was achieved by subtracting the basal surface of interest (SOI) from a trend surface (TS). The trend surface is generated by applying a median filter to the surface of interest. **b** Seismic section with marked surface of interest and trend surface. The detrended surface is shown in the box below the seismic profile. **c** Detrended surface showing examples of scours at the base of the Exmouth landslide. The inset to the right shows mapping polygons and associated oriented minimum bounding boxes used to extract morphometric parameters of the scours analysed. The image also shows sets of longitudinal and cross profiles utilised to assess the morphology of scours. See text for a detailed description of the data and methodologies implemented in the research

processing was applied to the landslide basal surfaces to create detrended outputs. The latter were subsequently analysed using GIS workflows in order to gain insights into the morphometric characteristics of basal scours (Fig. 4a).

## Seismic data

3D time-migrated seismic reflection data were depth-converted using a simple two-layer velocity model to account for the seawater velocity (1500 m/s) and for the Miocene to recent sediments (1700 m/s) (Fig. 3).

The dominant frequency of the seismic packages below the seabed reflection was calculated to be ~60 Hz. Assuming seabed sediment velocity of ~1550 m/s (Hengesh et al. 2012), the estimated seismic resolution for the shallow units where the landslides are imaged is ~6 m.

The seismic data were obtained from the National Offshore Petroleum Information Management System (NOPIMS; https://www.ga.gov.au/nopims) open repository. The Exmouth landslide was interpreted using the Bonaventure 3D dataset, whereas the Gorgon landslide was interpreted across the Draeck, Gorgon, and Acme 3D seismic surveys. Areas of poor imaging characterized by amplitude loss and artifacts are commonly observed at the overlapping edges of the seismic surveys (e.g. Fig. 5c).

## Detrending methodology

For the Gorgon case study, the interpreted surface of interest was the seabed that was mapped in three dimensions using the seismic data available. This is because the Gorgon landslide exhibits a fully evacuated headscarp; hence, the seabed coincides with the basal surface of the failure (Figs. 3 and 5).

For the Exmouth Plateau case study, the basal surface of the failure is buried beneath ~50 m of sediments (Figs. 3 and 6). This surface was also mapped using the available 3D seismic data in that location.

Seismic mapping was conducted using Halliburton DecisionSpace Desktop, following established 3D seismic interpretation workflows (e.g. Dorn 1998; Cartwright and Huuse 2005; Posamentier et al. 2007; Cox et al. 2020). Mapping was first carried out on a set of widely spaced profiles to guide subsequent automatic interpretation (i.e. autotracker; Dorn 1998) across the full 3D seismic volume and generation of continuous surfaces. Where necessary, additional manual mapping was performed in localised areas to infill gaps and ensure a fully continuous interpreted surface.

Once a surface of interest (SOI; i.e. basal surface) was mapped, a trend surface (TS; i.e. slope) was generated through the application of a standard median filter to the SOI (Fig. 4a). The median filter was calculated using the PowerCalculator tool within DecisionSpace Desktop. The filter operates by selecting a local neighbourhood of elevation points and assigning the median value to the central point of the neighbourhood. The optimal size of the median filter was

achieved by visually inspecting the result of multiple filtering iterations (Fig. 4b). The optimal results are achieved when the filtering produces a TS that resembles the overall bathymetric trend of SOI. The detrended surface (DS) was calculated through a simple subtraction of SOI from TS (i.e. DS = TS-SOI; Fig. 4a). In essence, this operation removes the effect of the trend imparted by the slope and exposes the detailed morphologies of the SOI. The DS surface would show negative and positive elevation values for points resting below and above the trend surface, respectively (Fig. 4b). In this work, the points below the TS (which correspond to scours) are color-coded in shades of blue, whereas the points above the TS are color-coded in shades of red (Fig. 4b and c). Detrending provides clear advantages over methods such as variance attribute (also known as coherence) and dip maps for highlighting geomorphic features in seismic data. Variance, which measures the similarity of adjacent seismic traces, is widely used to detect faults and erosional features (e.g. Chopra and Marfurt 2008). However, because the attribute relies on seismic amplitude variations, variance does not convey the morphological relief of the features investigated. Similarly, dip maps, which highlight gradient changes along a surface (e.g. Tibor et al. 2010), do not, unlike detrending, capture the three-dimensionality of features expressed along such surfaces.

## Morphometric analysis

Detrended surfaces were further analysed using standard GIS workflows in QGIS to extract key morphometric parameters of the scours (see; Figs. 4a, c and 7).

### Length and width of scours

The edge of scours was mapped using polygons (Fig. 4c). Edges were traced along the highest elevation points surrounding a scour (Fig. 4c). A standard, oriented minimum bounding box GIS algorithm was implemented. This allowed the creation of rectangles wrapping each scour (Fig. 4c). From these, the length and width of the scours were automatically extracted.

### Depth of scour erosion and volume of eroded material

Standard GIS zonal statistics workflows were implemented to calculate the depth of scours, which provide a magnitude of the erosional process that formed the scour. The statistics were calculated from the detrended surface using the same mapping polygons used to derive the length and width of scours. Since detrended values can vary across positive and negative values (Fig. 4b), a standard range algorithm was implemented to extract the depth of scours. Since the algorithm measures the range between the maximum and minimum values of the detrended surface within each scour mapping polygon, the resulting magnitude of depth of erosion should be considered a maximum estimate. The volume of eroded material for each scour was calculated by multiplying depth with the area of each scour. To expedite data gathering, the area of a scour was calculated as the area of the same oriented minimum bounding box used to derive the length and width of scours (see above). For this reason and given the fact that scours tend to taper at their terminations, their calculated area and volume might be overestimated (~20%).

### Slope gradient

A slope raster was computed from the trend surface using standard GIS workflows (TS; Fig. 4a). The slope raster was subsequently utilised to extract the mean slope gradient for each scour. This was achieved by implementing established GIS zonal statistics calculated within each scour's mapping polygon (Fig. 4c). This information provides insights into the overall slope gradient of the seabed where the scours occurred.

### Longitudinal and cross profiles

A series of longitudinal and cross profiles were created to evaluate the morphology of scours (Fig. 4c). Longitudinal profiles were traced following the scour axis. The cross profiles were taken perpendicular to the scour axis. For each scour, several cross profiles were taken at an interval of ~200 m between profiles. Both longitudinal and cross profiles were extracted from the detrended surfaces (DS; Fig. 4a).

# Results

Detrended basal surfaces of the Gorgon and Exmouth landslides are shown in Figs. 5 and 6, respectively. A statistical morphometric analysis of scours associated with the two landslides is presented in Fig. 7.

## Gorgon landslide

Detrended data of the Gorgon landslide show the presence of a prominent scour field ~25 km across that developed along the basal surface of this landslide (Fig. 5a). It is noted that the scour field is locally affected by a number of subcircular pockmarks, ~100 m across, either randomly distributed or organised in NW-oriented pockmarks trains (Fig. 5b and c).

Scours are mostly subparallel, trending NW–SE (Fig. 5a), with their lengths and widths ranging 1–5 km and 100 to 900 m, respectively (Figs. 5a, b, and 7a). The orientation of the scours is perpendicular to the landslide's headscarp, suggesting transport parallel to the scours' orientation (Fig. 5a). However, notably, the scours do not connect to the landslide headscarp, as most initiate ~5 km further downslope (Fig. 5a and c), suggesting that the onset of the process driving basal erosion is spatially detached from the locus of landslide evacuation.

Detailed examination of cross profiles reveals a pronounced asymmetry in the scour morphology. This is evident from the fact that scours exhibit a steep and a gentle flank attaining average dips of ~4° and ~2°, respectively (Figs. 5b and 7b). Depth of erosion along scours rarely exceeds 20 m (Fig. 5a). However, enhanced erosion might have occurred at the upslope termination of the scours, as suggested by the highest erosion depths observed in the longitudinal profiles at these locations (Fig. 7b).

Furthermore, combined analysis of the detrended basal surface and seismic profiles indicates that erosion along the scours diminished in areas where increased seabed gradients coincided with marked bathymetric breaks (Fig. 5c). In these locations, different sets of scours are observed to initiate downslope of these bathymetric breaks (Fig. 5c), suggesting a profound control of

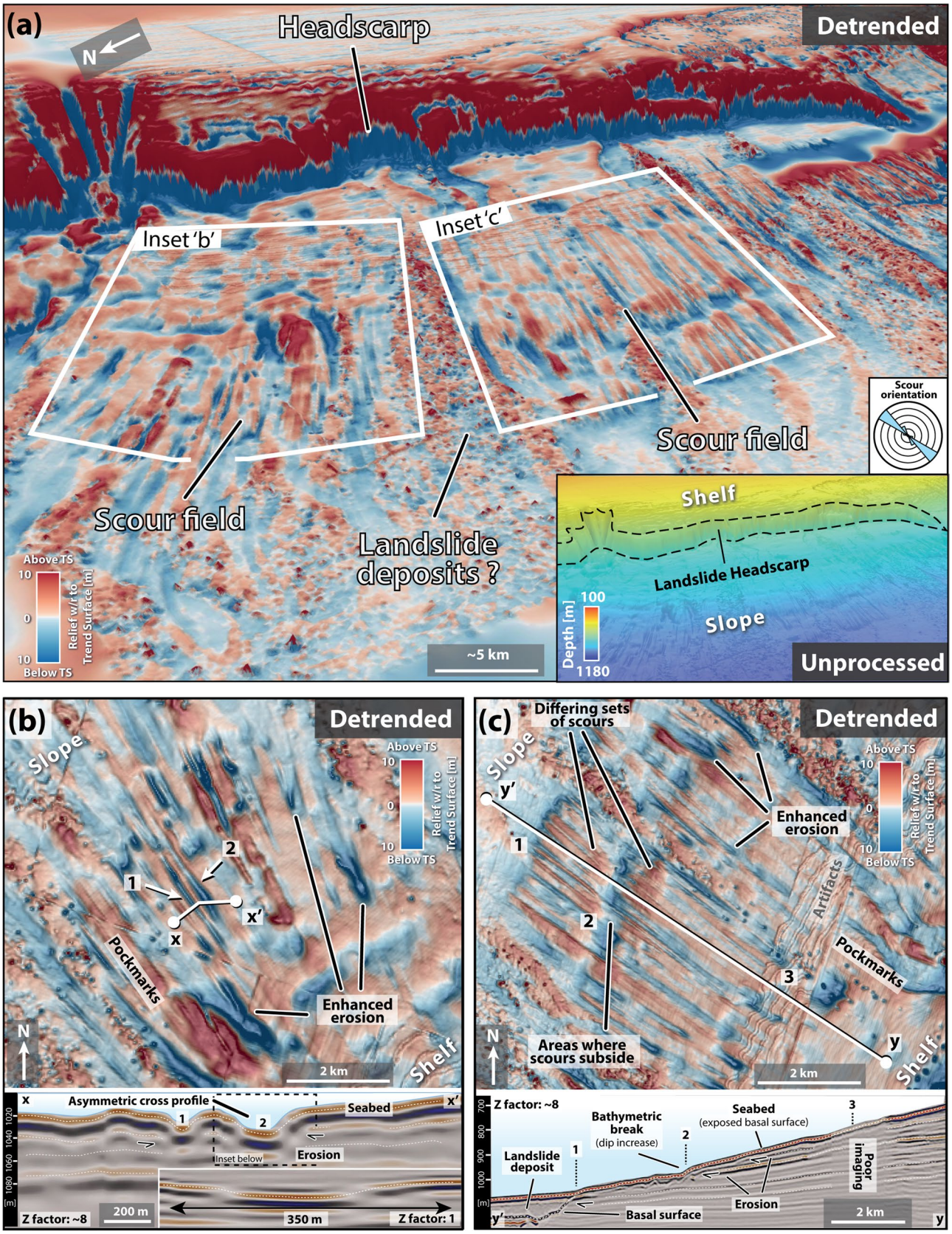
(a)
N
Headscarp
Detrended
Inset 'b'
Inset 'c'
Scour field
Scour orientation
Scour field
Landslide deposits ?
Above TS
10
0
10
Below TS
Relief w/r to Trend Surface [m]
~5 km
Shelf
Landslide Headscarp
Slope
100
Depth [m]
1180
Unprocessed
(b)
Detrended
Slope
Above TS
10
0
10
Below TS
Relief w/r to Trend Surface [m]
2
1
x'
x
Pockmarks
Enhanced erosion
N
2 km
Shelf
x
Asymmetric cross profile
1
2
Seabed
x'
Inset below
Erosion
1020
1040
1060
1080
[m]
Z factor: ~8
200 m
350 m
Z factor: 1
(c)
Differing sets of scours
Detrended
Slope
y'
Enhanced erosion
Above TS
10
0
10
Below TS
Relief w/r to Trend Surface [m]
1
Artifacts
2
Pockmarks
3
N
Areas where scours subside
2 km
y
Shelf
Z factor: ~8
Bathymetric break
(dip increase)
Seabed
(exposed basal surface)
Landslide deposit
1
2
3
Poor imaging
700
800
900
1000
[m]
y'
Basal surface
Erosion
2 km
y

◂**Fig. 5** **a** 3D view of the detrended seabed in the vicinity of the Gorgon landslide. The image shows prominent scour fields trending NW–SE. For comparison, unprocessed data is shown in the inset. **b**, **c** Closeup views of detrended data showing the details of the scour field. Insets at the bottom of the image show selected vertical seismic profiles highlighting the morphologies of scours. The location of the profiles is shown on the detrended maps (see text for detailed description of the data)

slope gradient on the effectiveness of the mechanism of erosion generating the Gorgon landslide scours.

### Exmouth landslide

The Exmouth landslide shows an arcuate headscarp ~10 km across followed by a constricted bottlenecked area ~2 km wide (Fig. 6a). Detrending of the basal surface reveals prominent crosscutting sets of diverging and converging scours indicating overall landslide transport to the SE (Fig. 6b). The diverging scours link back to the bottleneck indicating that remobilised materials were transported down the slope through this narrow feature (Fig. 6a). Vertical profiles show that the landslide body is ~100 m thick and is internally characterised by a chaotic seismic facies embedding numerous blocks resting on the basal surface (Fig. 6a and b). The blocks are commonly found at the downslope termination of scours and range in size from several tens of metres up to a few hundred metres, often exhibiting a triangular shape widening downwards toward the basal surface (Fig. 6a and c).

The diverging scours start incising the basal surface from the landslide headscarp and their length ranges from 250 to 10,000 m (Fig. 6b). These scours are twice as long as the longest scours of the Gorgon landslide (Figs. 5a, 6b, and 7a). The width of scours is similar to those of the Gorgon landslide (i.e., 70–1000 m). However, the depth of erosion of the Exmouth landslide scours is larger as they commonly exceed 15 m, with the deepest scours reaching a depth of 50 m (Figs. 6b and 7a). Longitudinal profiles of the Exmouth landslide scours markedly differ from those of the Gorgon Platforms. The former commonly display an increase in the depth of erosion towards the downslope termination of the scours (Figs. 6c and 7b), while the latter see the increase in the depth of erosion towards their upslope end (Fig. 7b). The cross profiles of the Exmouth landslide scours also differ from those of the Gorgon landslide as the former show symmetric and steeper flanks, with average flank dips of ~15°, while the latter exhibit shallower and asymmetric flanks (Fig. 7c).

### Correlation of morphometric parameters

The cross-correlation matrix in Fig. 7c explores potential correlation amongst scour morphometric parameters. Strikingly, the data show a poor correlation of slope gradient with any of the other morphometric parameters. There is, however, a noticeable separation of the range of slope gradients between the scours of the Exmouth and Gorgon landslides, with the latter restricted to slopes with gradients of 1–1.5° while the former found on a wider range of gradients up to 4° (Fig. 7a and c).

The matrix also shows correlation between the volume of eroded material by a scour with its width and depth of erosion, which is expected. It is also noticeable the correlation between length of scours and depth of erosion, as well as appreciable correlation between length of scours and volume eroded (Fig. 7c). However, strikingly, these correlations are observed only for Exmouth landslide scours (Fig. 7c).

## Discussion—formation of basal scours in submarine landslides

The dynamics of submarine landslides involve a range of processes that initiate with the detachment of material from the slope, typically occurring along a failure plane (e.g. Piper et al. 1985; Hampton et al. 1996; Moscardelli et al. 2006). Once evacuated, the failed mass may undergo rheological transformations through progressive disintegration and ingestion of seawater into the landslide body during its downslope transport (Masson et al. 2006; Talling et al. 2007). The initial movement often begins as a coherent block or series of blocks that transition into internally disorganised slumps and to gravity flows such as debris flows and turbidity currents (McHugh et al. 2002; Scarselli et al. 2022; Li et al. 2023). Across the spectrum of these transitions, seabed erosion is a common process that occurs at the base of the failures (Gee et al. 2007; Bull et al. 2009; Sobiesiak et al. 2018). In our study, application of trending workflows allows the unravelling of the detailed morphologies of basal scouring to provide insights into erosional processes associated with landslide emplacement.

### Downslope tooling due to sinking of landslide blocks (basal block tooling)

The chaotic and disrupted nature of the Exmouth landslide suggests that the deposits are internally disorganised, consistent with emplacement by slumping or debris-flow processes (Posamentier and Martinsen 2011; Scarselli 2020). Such cohesive, plastic modes of submarine slope movement are well known for their ability to transport large blocks as the deforming landslide mass moves downslope (Martinez et al. 2005; Jackson 2011; Nwoko et al. 2020). In the Exmouth landslide, large blocks are found to be lodged at the downslope termination of the scours (Fig. 6c). Their position suggests that these blocks may have eroded the sediments beneath and formed the scours as the landslide moved (Moscardelli et al. 2006; Ogata et al. 2012; Nwoko et al. 2020).

The downslope increase in erosion depth observed in this research along the Exmouth landslide scours (Fig. 7) may offer clues into block tooling dynamics. In this process, blocks detached from the landslide headwall and carried within the flow contribute to progressively greater erosion during a waning phase of collapse. In this scenario, as the landslide decelerates, blocks gradually sink to the base exerting increased erosion and eventually become lodged at the downslope termination of the resulting scours (Fig. 8). This might be related to potential block lifting mechanisms such as hydroplaning (Mohrig et al. 1998; De Blasio et al. 2004) and dispersive pressure (Bagnold 1954; Lowe 1982; Iverson 1997) becoming inefficient as landslides decelerate (Fig. 8).

The observed correlation between the length, width, depth of erosion and volume of eroded material for the Exmouth landslide scours (Fig. 7c) suggests that larger blocks are capable of generating larger scours, able to erode larger volumes of basal material. This is because transported blocks within submarine landslides are known

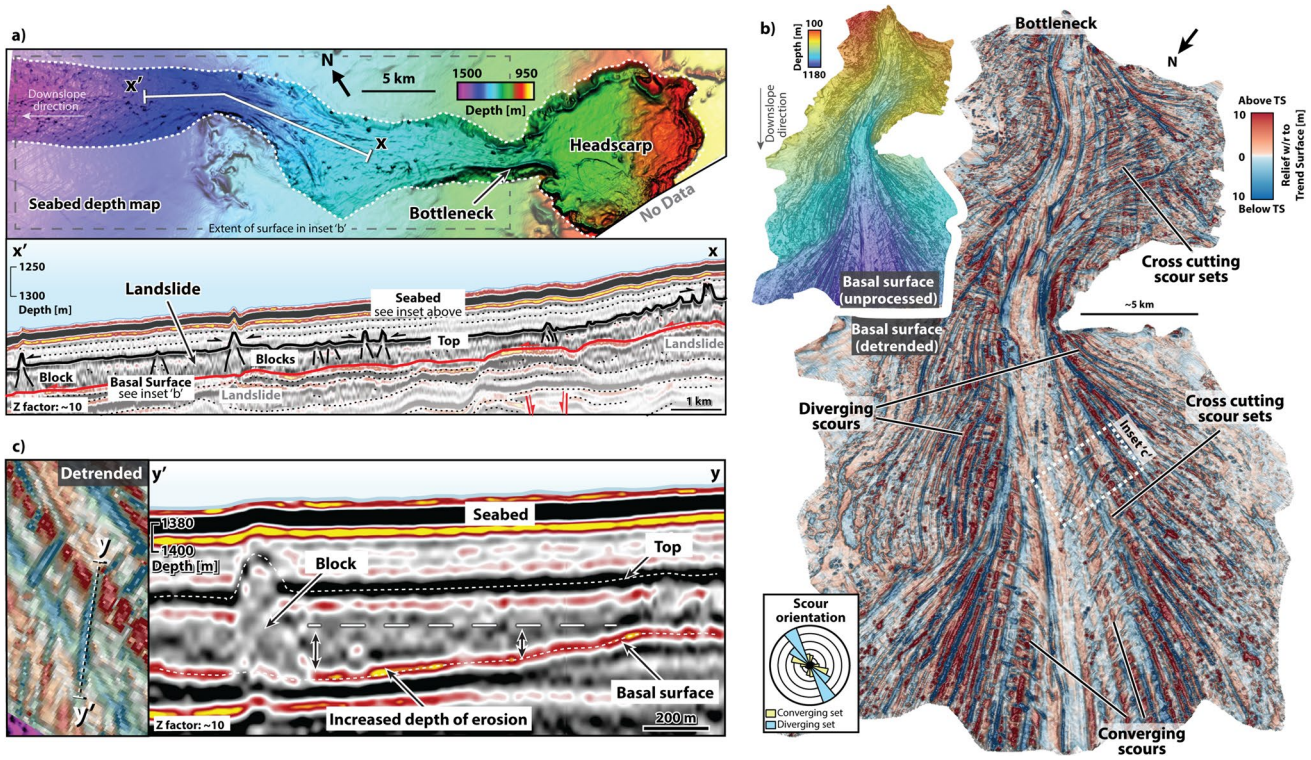


**Fig. 6** **a** Seabed map and key section showing the overall architecture of the Exmouth landslide. **b** Detrended data of the basal shear surface of the Exmouth landslide showing complex sets of scours. **c** Key seismic reflection profile along a scour showing the presence of ~150 m wide block lodged at the downdip termination of the scour. Also note the increase of the depth of the erosion toward the downslope termination of the scour

to mechanically degrade with transport (e.g. Hodgson et al. 2019; Nwoko et al. 2020; Wu et al. 2021). In this context, larger blocks (capable of generating wider scours) can withstand degradation for longer transport distances, enabling them to form longer and significantly more erosive scours (Fig. 8).

### Erosional scours induced by longitudinal flow vortices

The lack of correlation amongst length, width, and depth of erosion for the Gorgon scours (Fig. 7c) along with their distinct asymmetric and gentle flanks and their pronounced upslope erosion (Fig. 7b and c) suggests that these features may have formed through a mechanism not related to basal block tooling.

In flow dynamics, longitudinal vortices are known to develop as a result of flow instabilities (Swearingen and Blackwelder 1987; Forterre and Pouliquen 2001; Hall et al. 2008). In submarine environments, scour fields formed by elongated, parallel to sub-parallel, regularly spaced, erosional features are commonly documented in the literature (Coleman et al. 1981; Canals et al. 2006; Lastras et al. 2007; Puig et al. 2008). These scours are often attributed to the erosional action of helicoidal currents and, as such, exhibit their orientation parallel to flow direction (Allen 1969; Flood 1983, 1994; Bryant et al. 2001; Fedele and García 2009). Similarly, in subaerial environments, longitudinal flow vortices are believed to form scour fields at the base of glaciers, where they are associated with the runoff of subglacial meltwater in tunnel valleys (Lesemann et al. 2010, 2014), in addition to formation within pyroclastic flows (Kieffer and Sturtevant 1988; Kieffer et al. 2021). Planetary landscapes featuring elongated grooves and ridges have also been associated with the occurrence of longitudinal vorticity in fluid and granular flows (Thompson 1979; Carling et al. 2009; Magnarini et al. 2019).

We interpret the Gorgon landslide scours as features formed by the erosive action of helicoidal gravity flows generated from slope failures evacuated from the prominent headscarp observed upslope and to the SE of the scour field (Fig. 5a). Submarine landslides are well known to transition into sediment gravity currents due to downslope rheological transformations, driven by mechanical disaggregation and incorporation of ambient fluid into the failing mass (Fig. 8; Hampton 1972; Schwarz 1982; Piper et al. 1999; Dasgupta 2003; Strachan 2008; Piper and Normark 2009; Scarselli et al. 2022; Li et al. 2023). Along the Gorgon Platform, these transformations might have been favoured by the high velocity of the failing masses facilitated by the steep seabed slope (up to 15°; Fig. 3b) at the location of the landslide headscarp (Fig. 8). Transition to gravity currents might also be suggested by the fact that the Gorgon landslide lacks the abundance of coherent blocks observed in the Exmouth landslide (Figs. 5c and 6a).

In offshore continental margins, scours generated by helicoidal flows can reach widths in excess of 100 m and depths exceeding

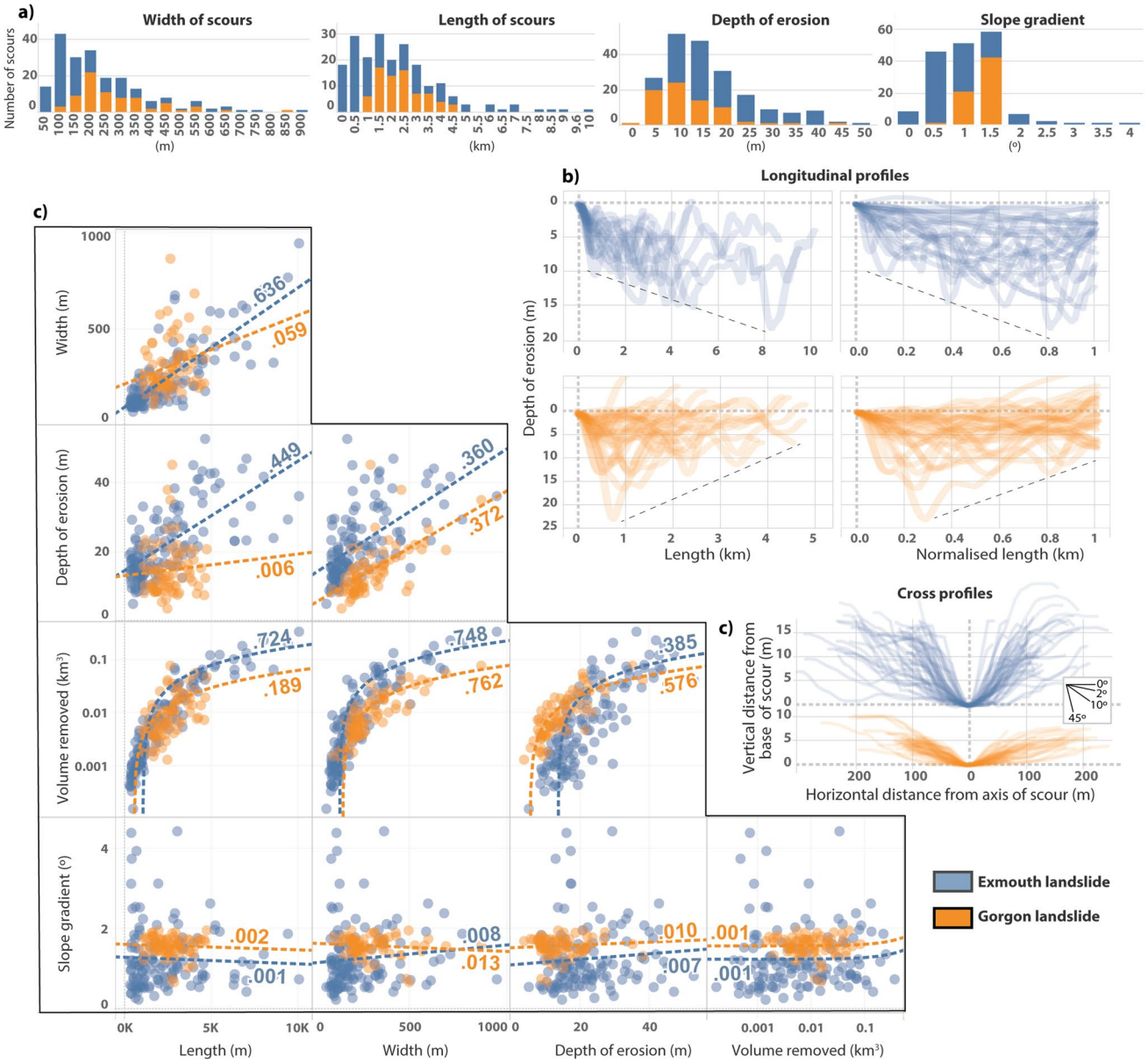


**Fig. 7** **a** Frequency histograms summarising the Exmouth and Gorgon landslides scour morphologies. **b** Stacked longitudinal and cross profiles of scours. **c** Cross correlation matrix of scours' parameters with $R^2$ values provided next to trend lines (see text for full discussion)

20 m (Flood 1983, 1994). These dimensions are consistent with the morphological parameters of the Gorgon landslide scours measured in this research (Fig. 7). Previous research suggests that the presence of substrate irregularities is required to focus flow erosion and promote onset of helicoidal flows and associated longitudinal scours (Flood 1983, 1994; Hall et al. 2008). In the case of the Gorgon landslide scours, the detrended data show the presence of circular seabed pockmarks located within the scour field (Fig. 5b and c). Provided that these formed before or during the evacuation of the Gorgon landslide, the pockmarks might have provided the roughness needed to promote initiation of helicoidal flows and scouring. The relative time of formation of the Gorgon landslides and the pockmarks is unknown. Pockmarks along the Gorgon Platform have been known to exist within and outside areas affected by landslides (Hengesh et al. 2012; Hengesh et al. 2013; Dirstein et al. 2013). Riera et al. (2022) suggested that the presence of pockmarks within landslide areas may indicate that interstitial fluids were mobilised and vented during, or shortly after, landslide emplacement, producing pockmarks either contemporaneously with, or immediately following, the mass-movement event. Pockmarks located outside the landslide area are unlikely to be related to landslide events. Fluid uplift and pockmark formation can be initiated by fault activity causing breaching of fluid reservoirs (e.g. Gay et al. 2007; Maia et al. 2016; Ruge et al.

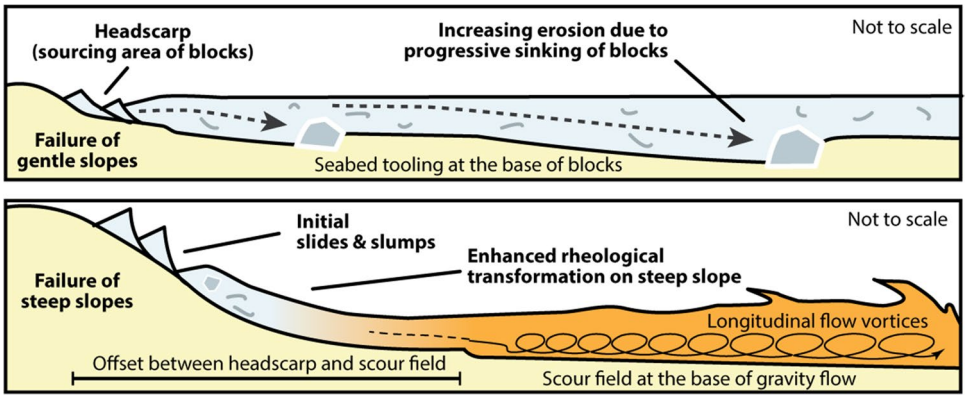


**Fig. 8** Schematic diagram for the formation of scours at the base of submarine landslides (see text for full discussion)

2021). In the Gorgon area, pockmarks are situated above major rift structures, including horsts that are known to form traps for gas accumulations in the Gorgon field (Riera et al. 2022). Reactivation of these structures prior to the emplacement of the Gorgon landslide and nearby failures cannot be excluded, as Miocene to present day reactivation of rift structures along the Northwest Shelf of Australia is well documented (Keep et al. 1998; Harrowfield et al. 2003; Harrowfield and Keep 2005; Keep et al. 2007; Keep et al. 2024). Evidence for interaction between the Gorgon landslide and pockmarks is supported by two observations: (1) the Gorgon landslide scours exhibit enhanced erosion at their upslope terminations (Figs. 5b, c and 7b), likely due to the presence of pockmarks promoting the initiation of helicoidal flows and localized scouring (Fig. 5b and c); and (2) landslide scours are predominantly found in areas where pockmarks are present (Fig. 5). In summary, it is plausible that these pockmarks were present before and/or during the emplacement of the Gorgon landslide, providing the seabed roughness necessary to promote the initiation of helicoidal flows and associated scours.

The Gorgon landslide scours bear strong resemblance to those formed by dilute pyroclastic density currents (Kieffer and Sturtevant 1988; Kieffer et al. 2021). In such flows, vorticity-associated scours occur as regularly spaced features arranged in extensive fields extending downslope from the flow origin (Kieffer et al. 2021), similar to the patterns revealed by detrending along the basal surface of the Gorgon landslide (Fig. 5). Another point of similarity is the cessation of the Gorgon landslide scours at bathymetric breaks (Fig. 5c), indicating that changes in slope gradient can strongly influence flow dynamics, suppressing longitudinal vortices and associated erosion. A comparable relationship between slope changes and vortex suppression has been documented for pyroclastic density currents (Kieffer et al., 2021) and attributed to the onset of large-scale turbulence as flows encounter changing gradients (Swearingen and Blackwelder 1987; Kieffer et al. 2021). These observations suggest that the flows responsible for the Gorgon landslide scours were likely low-density, analogous to dilute pyroclastic density currents, and that a similar slope-control mechanism may govern the stability of helicoidal flows and the suppression of scours in gravity-driven flows generated by submarine failures.

The Gorgon landslide scours also exhibited two distinct characteristics, namely (1) that the scours initiate ~5 km downslope from the landslide headscarp (Fig. 5); (2) the asymmetric shape of the scours observed on cross profiles (Fig. 7b). To explain the first observation, it is proposed that a sufficient landslide runout distance would be required to fully develop rheological transformations from a landslide to a sediment gravity flow (Fig. 8). Scarselli et al. (2022) provided geophysical evidence that complete transformation from a slump ~50 m thick into an accelerated, erosive flow occurred over a distance of up to 3 km. This, combined with the fact that generating flow vortices and related erosion requires current acceleration to velocities in excess of 30 cm/s (Flood 1994), could explain the spatial gap between the Gorgon landslide headscarp and the scour field further downslope (Fig. 8).

In submarine gravity currents, the Coriolis force acts at right angles to flow direction, altering the dynamics of these currents (e.g. Davarpanah Jazi et al. 2020). This effect is known to laterally deflect the bulk flow in submarine gravity currents (Davies et al. 2006; Wells 2009), causing observable asymmetry in the morphology of submarine channels systems (Cossu and Wells 2010; Cossu et al. 2010; Davarpanah Jazi et al. 2020). Laboratory experiments have shown that streamwise vorticity within bending channels is also affected by the Coriolis force, modifying erosional and depositional patterns along sinuous channels (Cossu et al. 2010). Although not supported by specific modelling effort, we infer that the Coriolis force might be able to perturb the symmetry of longitudinal vortices, resulting in laterally varying vortex strength and asymmetry in the scours they generate.

Along-slope bottom currents are also known to impact the dynamics of submarine gravity flow (e.g., Rodrigues et al. 2022). Flume tank experiments show that downslope gravity flows can be impacted by laterally impinging currents (Miramontes et al. 2020). This causes deviation of the downslope current and laterally varying erosional patterns at the base of the flow, producing asymmetric channels (Miramontes et al. 2020; Rodrigues et al. 2022). The NW Shelf of Australia, particularly the areas surrounding the Exmouth Plateau, has been influenced by intense bottom currents since the Late Jurassic (Wijeratne et al. 2018; Mantilla et al. 2022; Nugraha et al. 2022), suggesting that along-slope currents together with the effect of Coriolis cannot be excluded as factors that have caused the asymmetry of the morphology of the scours at the base of the Gorgon landslide. An alternative explanation for the

asymmetry of the scours is that unidirectional seafloor currents may have partially infilled the scour depressions with thin veneers of sediment. The thickness of such deposits would not be observed in seismic profiles because it is below the vertical resolution of the available seismic data.

## Key remarks and implications

In this study of submarine landslide dynamics, detrending applied to seismic data has proven to be a powerful tool able to remove broad slope trends and reveal enhanced morphologies previously not visible, therefore focusing on the mechanisms causing landslide evacuation and basal erosion. By applying this technique, new insights into the factors that control landslide dynamics can be gained to improve predictive models and enhance hazard assessments for regions prone to submarine landslides. Detrending was applied in this study to facilitate the recognition of erosional morphologies related to submarine landslides, enabling reconstruction of erosional dynamics and to discern two distinct genetic mechanisms of basal scouring (Fig. 8). Basal block tooling generates scours with symmetric and steep flanks that connect upslope to the source area of the blocks (i.e. headscarp). Increasing depth of erosion at the downslope termination of scours suggests that tooling is caused by substrate gouging as increased interaction of blocks with the seabed takes place at the base of a decelerating landslide. Width and length of scours might be intimately linked with the size of blocks embedded in a landslide. Larger blocks which are able to withstand degradation for longer distances during transport are capable of generating wide, long and erosive scours.

In contrast, elevated acceleration of failing masses on steep slopes favours downslope rheological transformation of landslides to gravity flows. Onset of longitudinal flow vortices promoted by the presence of seabed irregularities (i.e. pockmarks) can induce erosional scours with open flanks and spatially disconnected to the headscarp evacuating the initial landslide. Change in seabed slope gradient likely plays a crucial control on the stability of longitudinal flow vortices, causing scours to terminate where marked bathymetric breaks occur.

Being able to recognise these differing erosional morphologies allows reconstruction of failure dynamics and provides invaluable clues for a better understanding of the potential hazard posed by submarine landslides in offshore basins. In this research, detrending enabled enhancing the basal surface morphologies imaged with seismic data. This technique can be applied to any digital elevation model, supporting in-depth analysis across a wide range of marine, terrestrial, and planetary morphologies.


## Acknowledgements

Geoscience Australia is thanked for providing the seismic data utilised in this research. Esri and Halliburton are thanked for donating Royal Holloway with the academic licenses of ArcGIS Pro and DecisionSpace Desktop, respectively. Thanks to the QGIS Project Steering Committee for providing the open-source QGIS software. Salesforce is thanked for providing an academic licence of Tableau, which was utilised for the morphometric analysis of the data.


## Author contribution

Conceptualisation: NS, SC; methodology: NS; formal analysis and investigation: NS; writing—original draft preparation: NS; writing—review and editing: NS, SC, GM. All authors read and approved the final manuscript.


## Funding

GM gratefully acknowledges Science Technology Facilities Council (STFC) funding ST/Y001176/.


## Data availability

The primary seismic data utilised in this research are available through the National Offshore Petroleum Information Management System (NOPIMS) open repository https://www.ga.gov.au/nopims Derived data from seismic and GIS analysis are available upon request to the corresponding author.

## Declarations

**Conflict of interest** The authors declare no competing interests.



## References


Allen JRL (1969) Erosional current marks of weakly cohesive mud beds. J Sediment Res 39(2):607–623

Bagnold RA (1954) Experiments on a gravity-free dispersion of large solid spheres in a Newtonian fluid under shear. Proc R Soc Lond Ser A Math Phys Sci 225(1160):49–63

Bilal A, McClay K (2022) Tectonic and stratigraphic evolution of the central Exmouth Plateau, NW shelf of Australia. Mar Pet Geol 136:105447

Brigante R, Cencetti C, De Rosa P, Fredduzzi A, Radicioni F, Stoppini A (2017) Use of aerial multispectral images for spatial analysis of flooded riverbed-alluvial plain systems: the case study of the Paglia River (central Italy). Geomat Nat Hazards Risk 8(2):1126–1143

Bryant W, Bean D, Slowey N, Dellapenna T, Scott E (2001) Deepwater currents form mega-furrows near US Gulf's Sigsbee Escarpment. Offshore (Conroe, Tex) 61(7):94–95

Bull S, Cartwright J, Huuse M (2009) A review of kinematic indicators from mass-transport complexes using 3D seismic data. Mar Pet Geol 26:1132–1151. https://doi.org/10.1016/j.marpetgeo.2008.09.011

Butler RWH, Turner JP (2010) Gravitational collapse at continental margins: products and processes; an introduction. J Geol Soc London 167(3):569–570

Canals M, Puig P, de Madron XD, Heussner S, Palanques A, Fabres J (2006) Flushing submarine canyons. Nature 444(7117):354–357

Carling PA, Herget J, Lanz JK, Richardson K, Pacifici A (2009) Channel-scale erosional bedforms in bedrock and in loose granular

material: character, processes and implications. Megaflooding on Earth and Mars. Cambridge University Press, Cambridge, pp 13–32
Cartwright J, Huuse M (2005) 3D seismic technology: the geological 'Hubble.' Basin Res 17(1):1–20
Ceramicola S, Tinti S, Zaniboni F, Praeg D, Planinsek P, Pagnoni G, Forlin E (2014) Reconstruction and tsunami modeling of a submarine landslide on the Ionian margin of Calabria (Mediterranean sea). Proceedings of world landslide forum 3, 2–6 June 2014, Beijing. In: Landslide science for a safer geo environment: volume 3: targeted landslides. Springer, pp 557–562
Ceramicola S, Senatore MR, Cova A, Meo A, Forlin E, Critelli S, Markezic N, Zecchin M, Civile D, Bosman A, Candoni O, Casalbore D, Coste M, Cotterle D, Deponte M, Dominici R, Facchin L, Gordini E, Morelli E, Muto F, Praeg D, Romeo R, Chiocci FL (2024a) Geohazard features of the Gulf of Taranto. J Maps 20(1):2431073. https://doi.org/10.1080/17445647.2024.2431073
Ceramicola S, Cova A, Forlin E, Markezic N, Mangano G, Civile D, Zecchin M, Fanucci F, Colizza E, Corselli C, Morelli D, Savini A, Caburlotto A, Candoni O, Coste M, Cotterle D, Critelli S, Cuppari A, Deponte M, Dominici R, Facchin L, Gordini E, Locatelli M, Muto F, Praeg D, Romeo R, Tessarolo C (2024b) Geohazard features of the ionian calabrian margin. J Maps 20(1). https://doi.org/10.1080/17445647.2024.2349785
Chopra S, Marfurt KJ (2008) Emerging and future trends in seismic attributes. Lead Edge 27(3):298–318
Coleman JM, Prior DB, Adams CE (1981) Erosional furrows on continental shelf edge, Mississippi delta region. Geo-Mar Lett 1:11–15
Cossu R, Wells MG (2010) Coriolis forces influence the secondary circulation of gravity currents flowing in large-scale sinuous submarine channel systems. Geophys Res Lett 37:L17603. https://doi.org/10.1029/2010GL044296
Cossu R, Wells MG, Wåhlin AK (2010) Influence of the Coriolis force on the velocity structure of gravity currents in straight submarine channel systems. J Geophys Res 115:C11016
Cox DR, Newton AM, Huuse M (2020) An introduction to seismic reflection data: Acquisition, processing and interpretation. In: Scarselli N, Adam J, Chiarella D, Roberts DG, Bally AW (eds) Regional Geology and Tectonics. Volume 1: Principles of Geologic Analysis, 2nd edn. Elsevier, pp 571–603
Dakin N, Pickering KT, Mohrig D, Bayliss NJ (2013) Channel-like features created by erosive submarine debris flows: field evidence from the Middle Eocene Ainsa Basin, Spanish Pyrenees. Mar Pet Geol 41:62–71
Dasgupta P (2003) Sediment gravity flow—the conceptual problems. Earth Sci Rev 62:265–281. https://doi.org/10.1016/S0012-8252(02)00160-5
Davarpanah Jazi S, Wells MG, Peakall J, Dorrell RM, Thomas RE, Keevil GM et al (2020) Influence of Coriolis force upon bottom boundary layers in a large-scale gravity current experiment: implications for evolution of sinuous deep-water channel systems. J Geophys Res Oceans 125:e2019JC015284. https://doi.org/10.1029/2019JC015284
Davies PA, Wåhlin AK, Guo Y (2006) Laboratory and analytical model studies of the Faroe Bank Channel deep-water outflow. J Phys Oceanogr 36(7):1348–1364
De Blasio FV, Engvik L, Harbitz CB, Elverhøi A (2004) Hydroplaning and submarine debris flows. J Geophys Res Oceans 109:C01002. https://doi.org/10.1029/2002JC001714
Dirstein JK, Hengesh JV, Stanley AJ (2013) Identification of fluid flow features in the seafloor and subsurface and their implications for prospect and geohazard assessment: examples from the Australian Northwest Shelf. In: Keep, M., Moss, S.J. (Eds.), The Sedimentary Basins of Western Australia IV: Proceedings of the Petroleum Exploration Society of Australia Symposium, Perth, WA
Dorn GA (1998) Modern 3-D seismic interpretation. Lead Edge 17(9):1262–1262
Draganits E, Schlaf J, Grasemann B, Argles T (2008) Giant submarine landslide grooves in the Neoproterozoic/Lower Cambrian Phe Formation, northwest Himalaya: mechanisms of formation and palaeogeographic implications. Sediment Geol 205(3–4):126–141
Fedele JJ, García MH (2009) Laboratory experiments on the formation of subaqueous depositional gullies by turbidity currents. Mar Geol 258(1–4):48–59
Flood RD (1983) Classification of sedimentary furrows and a model for furrow initiation and evolution. Geol Soc Am Bull 94(5):630–639
Flood RD (1994) Abyssal bedforms as indicators of changing bottom current flow: examples from the US East Coast continental rise. Paleoceanography 9(6):1049–1060
Forterre Y, Pouliquen O (2001) Longitudinal vortices in granular flows. Phys Rev Lett 86(26):5886
Frey-Martínez J, Bertoni C, Gérard J, Matías H (2011) Processes of submarine slope failure and fluid migration on the Ebro continental margin: implications for offshore exploration and development, in Shipp, R.G., Weimer P. & Posamentier H.R. (Eds), Mass-transport deposits in deepwater settings. SEPM Special Publications, 96, 181–198
Gay A, Lopez M, Berndt C, Seranne M (2007) Geological controls on focused fluid flow associated with seafloor seeps in the Lower Congo basin. Mar Geol 244(1–4):68–92
Gee MJR, Uy HS, Warren J, Morley CK, Lambiase JJ (2007) The Brunei slide: a giant submarine landslide on the North West Borneo margin revealed by 3D seismic data. Mar Geol 246(1):9–23
Haas TD, Woerkom TV (2016) Bed scour by debris flows: experimental investigation of effects of debris-flow composition. Earth Surf Process Landforms 41(13):1951–1966
Hall B, Meiburg E, Kneller B (2008) Channel formation by turbidity currents: Navier–Stokes-based linear stability analysis. J Fluid Mech 615:185–210
Hampton MA (1972) The role of subaqueous debris flow in generating turbidity currents. J Sediment Res 42:775–793
Hampton MA, Lee HJ, Locat J (1996) Submarine landslides. Rev Geophys 34(1):33–59
Harbitz CB, Løvholt F, Bungum H (2014) Submarine landslide tsunamis: how extreme and how likely? Nat Hazards 72:1341–1374
Harrowfield M, Keep M (2005) Tectonic modification of the Australian North-West Shelf: episodic rejuvenation of long-lived basin divisions. Basin Res 17:225–239. https://doi.org/10.1111/j.1365-2117.2005.00251.x
Harrowfield M, Cunneen J, Keep M, Crowe W (2003) Early-stage orogenesis in the Timor Sea region, NW Australia. J Geol Soc London 160:991–1002
Hengesh J, Dirstein J, Stanley A (2012) Seafloor geomorphology and submarine landslide hazards along the continental slope in the Carnarvon basin, Exmouth plateau, North West Shelf, Australia. APPEA J 52:493–511
Hengesh JV, Dirstein JK, Stanley AJ (2013) Landslide geomorphology along the Exmouth plateau continental margin, North West Shelf, Australia. Aust Geomech 48:71–92
Hodgson DM, Brooks HL, Ortiz-Karpf A, Spychala Y, Lee DR, Jackson CL (2019) Entrainment and abrasion of megaclasts during submarine landsliding and their impact on flow behaviour. Geological Society, London, Special Publications 477(1):223–240
Iverson RM (1997) The physics of debris flows. Rev Geophys 35(3):245–296
Jackson CA (2011) Three-dimensional seismic analysis of megaclast deformation within a mass transport deposit; implications for debris flow kinematics. Geology 39(3):203–206
Keep M, Powell CM, Baille PW (1998) Neogene deformation of the North West Shelf, Australia. In: Purcell, P.G. and Purcell, R.R. (eds) The Sedimentary Basins of Western Australia 2. Proceedings of the Petroleum Exploration Society of Australia Symposium, Perth, 81–91
Keep M, Harrowfield M, Crowe W (2007) The Neogene tectonic history of the North West Shelf, Australia. Explor Geophys 38:151–174

Keep M, Lindhorst K, Kuhnt W, Holbourn A (2024) Using shallow hydroacoustic data to image seafloor mass transport deposits on the North West Shelf of Australia: links to neotectonics. Geological Society, London, Special Publications 525(1):269–285
Kieffer SW, Sturtevant B (1988) Erosional furrows formed during the lateral blast at Mount St. Helens, May 18, 1980. J Geophys Res Solid Earth 93(B12):14793–14816
Kieffer SW, Meiburg E, Best J, Austin J (2021) The mysterious grooves of Volcán Bárcena: a review of the role of streamwise counter-rotating vortices during erosion by dilute pyroclastic density currents. Bull Volcanol 83(4):26
Lastras G, Canals M, Urgeles R, Amblas D, Ivanov M, Droz L, Dennielou B, Fabrés J, Schoolmeester T, Akhmetzhanov A, Orange D (2007) A walk down the Cap de Creus canyon, Northwestern Mediterranean Sea: recent processes inferred from morphology and sediment bedforms. Mar Geol 246(2–4):176–192
Lesemann JE, Piotrowski JA, Wysota W (2010) Glacial curvilineations": new glacial landforms produced by longitudinal vortices in subglacial meltwater flows. Geomorphology 120(3–4):153–161
Lesemann JE, Piotrowski JA, Wysota W (2014) Genesis of the 'glacial curvilineation' landscape by meltwater processes under the former Scandinavian Ice Sheet, Poland. Sediment Geol 312:1–18
Li Y, Dong Y, Chen G (2023) A numerical investigation of transformation rates from debris flows to turbidity currents under shearing mechanisms. Appl Sci 13(7):4105
Liu X, Wang Y, Zhang H, Guo X (2023) Susceptibility of typical marine geological disasters: an overview. Geoenviron Disasters 10(1):10
Longley IM, Buessenschuett C, Clydsdale L, Cubitt CJ, Davis RC, Johnson MK, Marshall NM, Murray AP, Somerville R, Spry TB, Thompson NB (2002) The North West shelf of Australia–a woodside perspective. The Sedimentary Basins of Western Australia 3: Proceedings of the Petroleum Exploration Society of Australia Symposium, Perth (2002), pp. 27–88
Løvholt F, Pedersen G, Harbitz CB, Glimsdal S, Kim J (2015) On the characteristics of landslide tsunamis. Philos Trans R Soc Lond A Math Phys Eng Sci 373:20140376. https://doi.org/10.1098/rsta.2014.0376
Lowe DR (1982) Sediment gravity flows; II, Depositional models with special reference to the deposits of high-density turbidity currents. J Sediment Res 52(1):279–297
Lu H, Shipp C (2011) Impact of a large mass-transport deposit on a field development in the upper slope of southwestern Sabah, Malaysia, offshore northwest Borneo, in Shipp R.G., Weimer, P. & Posamentier, H.R. (Eds), Mass-transport deposits in deepwater settings: SEPM Special Publications Editors, SEPM Special Publication 96 pp. 199–218
Mangano G, Ceramicola S, Alves TM, Zecchin M, Civile D, Del Ben A, Critelli S (2023) A new large-scale gravitational complex discovered in the Gulf of Squillace (central Mediterranean): tectonic implications. Sci Rep 13(1):14695
Martinez JF, Cartwright J, Hall B (2005) 3D seismic interpretation of slump complexes: examples from the continental margin of Israel. Basin Res 17(1):83–108
Masson DG, Harbitz CB, Wynn RB, Pedersen G, Løvholt F (2006) Submarine landslides: processes, triggers and hazard prediction. Philos Trans R Soc A Math Phys Eng Sci 364:2009–2039
McCormack KD, McClay K (2013) Structural architecture of the Gorgon Platform, North West Shelf, Australia. In: Keep, M., Moss, S.J. (Eds.), The Sedimentary Basins of Western Australia IV: Proceedings of the Petroleum Exploration Society of Australia Symposium, Perth, WA
McHugh CMG, Damuth JE, Mountain GS (2002) Cenozoic mass-transport facies and their correlation with relative sea-level change, New Jersey continental margin. Mar Geol 184:295–334. https://doi.org/10.1016/S0025-3227(01)00240-7
Magnarini G, Mitchell TM, Grindrod PM, Goren L, Schmitt HH (2019) Longitudinal ridges imparted by high-speed granular flow mechanisms in martian landslides. Nat Commun 10(1):4711
Maia AR, Cartwright J, Andersen E (2016) Shallow plumbing systems inferred from spatial analysis of pockmark arrays. Mar Pet Geol 77:865–881
Mantilla O, Hernández-Molina FJ, Scarselli N (2022) Can deepwater bottom currents generate clinothems? An example of a large, asymmetric mounded drift in Upper Jurassic to Lower Cretaceous sediments from northwestern Australia. Geology 50(6):741–745
Miramontes E, Eggenhuisen JT, Jacinto RS, Poneti G, Pohl F, Normandeau A, Calvin Campbell D, Hernández-Molina FJ (2020) Channel-levee evolution in combined contour current–turbidity current flows from flume-tank experiments. Geology 48(4):353–357
Mohrig D, Ellis C, Parker G, Whipple KX, Hondzo M (1998) Hydroplaning of subaqueous debris flows. Geol Soc Am Bull 110(3):387–394
Moscardelli L, Wood L, Mann P (2006) Mass-transport complexes and associated processes in the offshore area of Trinidad and Venezuela. AAPG Bull 90(7):1059–1088
Nissen SE, Haskell NL, Steiner CT, Coterill KL (1999) Debris flow outrunner blocks, glide tracks, and pressure ridges identified on the Nigerian continental slope using 3-D seismic coherency. Lead Edge 18(5):595–599
Nugraha HD, Jackson CAL, Johnson HD, Hodgson DM, Reeve MT (2019) Tectonic and oceanographic process interactions archived in late Cretaceous to present deep-marine stratigraphy on the Exmouth Plateau, offshore NW Australia. Basin Res 31(3):405–430
Nugraha HD, Jackson CAL, Johnson HD, Hodgson DM, Clare MA (2022) Extreme erosion by submarine slides. Geology 50(10):1130–1134
Nwoko J, Kane I, Huuse M (2020) Megaclasts within mass-transport deposits: their origin, characteristics and effect on substrates and succeeding flows. Geological Society, London, Special Publications 500(1):515–530
Ogata K, Mutti E, Pini GA, Tinterri R (2012) Mass transport-related stratal disruption within sedimentary mélanges: examples from the northern Apennines (Italy) and south-central Pyrenees (Spain). Tectonophysics 568:185–199
Ogata K, Festa A, Pini GA (2019) Submarine landslides: subaqueous mass transport deposits from outcrops to seismic profiles, vol 247. Wiley
Ols C, Klesse S, Girardin MP, Evans ME, DeRose RJ, Trouet V (2023) Detrending climate data prior to climate–growth analyses in dendroecology: a common best practice? Dendrochronologia 79:126094
Piper DJW, Shor AN, Farre JA, O'Connell S, Jacobi R (1985) Sediment slides and turbidity currents on the Laurentian Fan: sidescan sonar investigations near the epicenter of the 1929 Grand Banks earthquake. Geology 13:538
Piper DJ, Cochonat P, Morrison ML (1999) The sequence of events around the epicentre of the 1929 Grand Banks earthquake: initiation of debris flows and turbidity current inferred from sidescan sonar. Sedimentology 46:79–97
Piper DJ, Normark WR (2009) Processes that initiate turbidity currents and their influence on turbidites: a marine geology perspective. J Sediment Res 79(6):347–362
Posamentier HW, Kolla V (2003) Seismic geomorphology and stratigraphy of depositional elements in deep-water settings. J Sediment Res 73(3):367–388
Posamentier HW, Davies RJ, Cartwright JA, Wood L (2007) Seismic geomorphology – an overview. In: Davies R.J., Posamentier H.W. & Wood L.J. (eds) Seismic Geomorphology: Applications to Hydrocarbon Exploration and Production. Geological Society, London, Special Publications, 277, pp. 1–14

Posamentier HW, Martinsen OJ (2011) The character and genesis of submarine mass-transport deposits: insights from outcrop and 3D seismic data. In: Shipp, R.C., Posamentier, H.W. (Eds.), Mass-Transport Deposits in Deepwater Settings, SEPM Special Publication, 96, pp. 7 38

Prior DB, Bornhold BD, Johns MW (1984) Depositional characteristics of a submarine debris flow. J Geol 92(6):707–727

Puig P, Palanques A, Orange DL, Lastras G, Canals M (2008) Dense shelf water cascades and sedimentary furrow formation in the Cap de Creus Canyon, northwestern Mediterranean Sea. Cont Shelf Res 28(15):2017–2030

Ramalho I, Omira R, Terrinha P (2024) Tsunami hazard induced by a submarine landslide in the Tagus delta off Lisbon (Portugal). Nat Hazards. https://doi.org/10.1007/s11069-024-07045-7

Riera R, Paumard V, de Gail M, Saqab MM, Lebrec U, Lang SC, Lane A (2022) Origin of seafloor pockmarks overlying submarine landslides: insights from semi-automated mapping of 3D seismic horizons (North West Shelf, Australia). Mar Pet Geol 136:105453

Rodrigues S, Hernández-Molina FJ, Fonnesu M, Miramontes E, Rebesco M, Campbell DC (2022) A new classification system for mixed (turbidite-contourite) depositional systems: examples, conceptual models and diagnostic criteria for modern and ancient records. Earth-Sci Rev 230:104030

Ruge SM, Scarselli N, Bilal A (2021) 3D seismic classification of fluid escape pipes in the western Exmouth Plateau, North West Shelf of Australia. J Geol Soc London 178(3):jgs2020-096

Scarselli N, McClay K, Elders C (2013) Submarine slide and slump complexes, Exmouth Plateau, NW Shelf of Australia. In: Keep, M., Moss S.J. (Eds.), The Sedimentary Basins of Western Australia IV: Proceedings of the Petroleum Exploration Society of Australia Symposium, Perth, WA

Scarselli N (2020) Submarine landslides - architecture, controlling factors and environments. A summary. In: Scarselli, N., Adam, J., Chiarella, D., Roberts, D.G. and Bally, A.W. (eds) Regional Geology and Tectonics. Volume 1: Principles of Geologic Analysis, 2nd edn. Elsevier, 417–439.

Scarselli N, McClay K, Elders C (2020) Composite slope failures: seismic examples from the NW Shelf of Australia. In: Ogata K, Festa A, Pini GA (eds) Submarine Landslides: Subaqueous Mass-Transport Deposits from Outcrops to Seismic Profiles, American Geophysical Union, Geophysical Monograph. John Wiley & Sons Inc, pp 261–276

Scarselli N, McClay K, Elders C (2022) Regional assessment of gravity-driven deformation offshore Namibia (West Africa)—styles, distribution and controlling factors. Basin Res 34(6):2013–2041

Schwarz HU (1982) Subaqueous slope failures — experiments and modern occurrences. Contributions to Sedimentary Geology, 11, Schweizerbart, Stuttgart, p 116

Sobiesiak MS, Kneller B, Alsop GI, Milana JP (2018) Styles of basal interaction beneath mass transport deposits. Mar Pet Geol 98:629–639

Strachan LJ (2008) Flow transformations in slumps: a case study from the Waitemata Basin, New Zealand. Sedimentology 55:1311–1332

Swearingen JD, Blackwelder RF (1987) The growth and breakdown of streamwise vortices in the presence of a wall. J Fluid Mech 182:255–290

Talling PJ, Wynn RB, Masson DG, Frenz M, Cronin BT, Schiebel R et al (2007) Onset of submarine debris flow deposition far from original giant landslide. Nature 450(541):544. https://doi.org/10.1038/nature06313

Tanabe J, Miller D, Tregellas J, Freedman R, Meyer FG (2002) Comparison of detrending methods for optimal fMRI preprocessing. Neuroimage 15(4):902–907

Tappin DR (2021) Submarine landslides and their tsunami hazard. Annu Rev Earth Planet Sci 49(1):551–578

Thompson DE (1979) Origin of longitudinal grooving in Tiu Vallis-Mars: isolation of responsible fluid-types. Geophys Res Lett 6(9):735–738

Tibor G, Niemi TM, Ben-Avraham Z, Al-Zoubi A, Sade RA, Hall JK, Al-Ruzouq R (2010) Active tectonic morphology and submarine deformation of the northern Gulf of Eilat/Aqaba from analyses of multibeam data. Geo-Mar Lett 30(6):561–573

Toniolo H, Harff P, Marr J, Paola C, Parker G (2004) Experiments on reworking by successive unconfined subaqueous and subaerial muddy debris flows. J Hydraul Eng 130(1):38–48

Urgeles R, Bahk J-J, Lee S-H, Horozal S, Cukur D, Kim S-P, Kim G-Y, Jeong S-W, Um I-K (2019) Tsunami hazard from submarine landslides: scenario-based assessment in the Ulleung Basin, East Sea (Japan Sea). Geosci J 23:439–460. https://doi.org/10.1007/s12303-018-0044-x

Wang F, Dai Z, Nakahara Y, Sonoyama T (2018) Experimental study on impact behavior of submarine landslides on undersea communication cables. Ocean Eng 148:530–537

Watson MW (1986) Univariate detrending methods with stochastic trends. J Monet Econ 18(1):49–75

Wells MG (2009) How Coriolis forces can limit the spatial extent of sediment deposition of a large-scale turbidity current. Sediment Geol 218(1–4):1–5

Wijeratne S, Pattiaratchi C, Proctor R (2018) Estimates of surface and subsurface boundary current transport around Australia. J Geophys Res Oceans 123(5):3444–3466

Winata M, Elders C, Maselli V, Stephenson RA (2023) Regional seismic stratigraphic framework and depositional history of the post-Valanginian passive margin sequences in the Northern Carnarvon Basin, North West Shelf of Australia. Mar Pet Geol 156:106418

Wu Z, Huang NE, Long SR, Peng CK (2007) On the trend, detrending, and variability of nonlinear and nonstationary time series. Proc Natl Acad Sci U S A 104(38):14889–14894

Wu N, Jackson CAL, Johnson HD, Hodgson DM, Clare MA, Nugraha HD, Li W (2021) The formation and implications of giant blocks and fluid escape structures in submarine lateral spreads. Basin Res 33(3):1711-1730.a

Wu N, Jackson CAL, Clare MA, Hodgson DM, Nugraha HD, Steventon MJ, Zhong G (2023) Diagenetic priming of submarine landslides in ooze-rich substrates. Geology 51(1):85–90

Zhang S, Ma Y, Chen F, Liu J, Chen F, Lu S, Jiang L, Li D (2020) A new method for supporting interpretation of paleochannels in a large scale—detrended Digital Elevation Model interpretation. Geomorphology 369:107374



**Nicola Scarselli (✉)**
Royal Holloway University of London, Department of Earth Sciences, Egham, Surrey, UK
Email: nicola.scarselli@rhul.ac.uk

**Silvia Ceramicola**
National Institute of Oceanography and Applied Geophysics-OGS, Trieste, Italy

**Giulia Magnarini**
Natural History Museum, London, UK

**Giulia Magnarini**
Laboratoire de Planétologie et Géosciences, Nantes Université, CNRS UMR, Nantes 6112, France